ISSN: 1976-7277

# Quality Assessment of Color Normalization Method by Similarity Index Metrics- A Comparative Study for Histopathology Images

Rubina Akter Rabeya<sup>1</sup>, Nam Hoon Cho<sup>2</sup>, Hee-Cheol Kim<sup>1\*</sup>, Heung-Kook Choi<sup>3\*</sup>

<sup>1</sup> Department of Digital Anti-Aging Healthcare, Inje University Gimhae 50834, Korea

[e-mail: rubinatr20@gmail.com, heeki@inje.ac.kr]

<sup>2</sup> Department of Pathology, Severance Hospital, Yonsei University Seoul 03722, Korea

[e-mail: cho1988@yumc.yonsei.ac.kr]

<sup>3</sup> Department of Computer Engineering, Inje University Gimhae 50834, Korea

[e-mail: cschk@inje.ac.kr]

\*Corresponding author: Hee-Cheol Kim, Heung-Kook Choi

Received August 19, 2024; revised March 28, 2025; accepted April 20, 2025; published May 31, 2025

#### Abstract

One of the biggest challenges of histopathology image processing is to preserve structural similarity while processing for further research. Color normalization algorithms can play a significant role in preserving the structure of histopathology images from various standpoints. In this research, we provide a comparative analysis of seven distinct color normalization algorithms by evaluating three state-of-the-art structural similarity index metrics often employed in image processing. 100 malignant prostate cancer histopathology tissue images (256 × 256) from various grading (Gleason score 3, 4, and 5) have been utilized here. The structure similarity index matrix (SSIM), quaternion structure similarity index matrix (QSSIM), and multi-scale structure similarity index matrix (MS-SSIM) are three state-of-theart quality evaluation metrics used in this research. Also, by computing the mean standard deviation (SD) of the grayscale images to determine the noise level and signal-to-noise ratio (SNR), respectively, we examined six denoising algorithms with various parameters to improve the efficacy of this analysis. This study provides a higher value for each of the threesimilarity metrics, indicating a relatively superior performance for the Blind Color Decomposition algorithm. Furthermore, the Gaussian algorithm outperforms the six denoising techniques in terms of SNR and SD. When we integrated the Blind Color Decomposition and Gaussian algorithm with our experimented specific parameters, we were able to obtain the

This research was supported by a grant from the Korea Health Technology R&D Project through the Korea Health Industry Development Institute validation (KHIDI), funded by the Ministry of Health & Welfare, Republic of Korea (Grant No: HI21C0977); National Research Foundation of Korea (NRF) grant funded by the Korea government (MIST) (Grant No. 2021R1A2C2008576), and supported by the MSIT (Ministry of Science ICT), Korea, under the National Program for Excellence in SW, supervised by the IITP(Institute of Information & Communications Technology Planning & Evaluation) in 2022 (2022-0-01091, 1711175863).

ultimate higher value for all three structural similarity index metrics. We anticipate that this analysis will have a substantial impact on various aspects of histopathology image processing, including segmentation, classification, feature extraction, and the creation of novel algorithms.

**Keywords:** Color normalization, Denoising, Histopathology, Structural similarity, Image analysis.

# 1. Introduction

Color variation in histopathology images gives histopathologists various advantages when analyzing critical information for further diagnosis of cancerous tissue. Color diversity in histopathology images occurs because of the use of various microscopic scanners, staining solutions, and staining techniques, which is a broad area of research nowadays for both pathologists and researchers to aim for early and accurate diagnosis [1]. One of the most frequently used techniques in histopathology image processing is to utilize various colornormalizing algorithms to assess these color variations. Researchers have created various color normalization techniques over the years, each with unique advantages and drawbacks, but one of the most difficult issues is preserving the fine details and structural similarity of histopathological images after normalization. Even so, due to these various recording devices, images contain some random noise during image acquisition which tends to introduce artifacts and eliminate small features from the histopathological image [2]. To lessen noise from images while improving image quality and maintaining fine structure features, several denoising techniques have also been introduced in the field of histopathology image analysis. While it has been suggested that converting RGB to grayscale can reduce color variance, doing so also results in information loss [3-5]. Therefore, it may be more efficient to use color normalization and denoising algorithms to lessen noise and color variations. We implemented seven color normalization algorithms, including histogram specification [6], min-max normalization [7], complete color normalization [8], blind color decomposition [9], contrast enhancement (CLAHE) [10, 11], color deconvolution [12], and macenko [13] to make a comparative quality assessment of histopathology images, with a primary concern of analyzing the structural similarity from various aspects of a histopathology image. Also, we implemented six imagedenoising techniques including a median [14], gaussian [14, 15], bilateral [15], wavelet [16], non-local means [17], and mean filter [14] as well. The standard quality evaluation matrix has been utilized to assess the structural similarity of all the approaches employed in our study using images with varying Gleason scores from a prostate cancer dataset [18]. The following is a summary of the key findings and contributions of this paper.

(1) Implement seven different color normalization techniques to lower color variation and improve quality to analyze the structural similarity of the histopathological prostate cancer images. Additionally, apply six distinct image-denoising techniques to lower the noise level while maintaining the images' fine features. We also outline each method's primary benefits and drawbacks.

- (2) We employ three state-of-the-art structural similarity evaluation metrics, namely the structure similarity index matrix (SSIM), the quaternion structure similarity index matrix (QSSIM), and the multi-scale structure similarity index matrix (MS-SSIM), to perform a comparative analysis of the qualitative effects of each color normalization method on our dataset.
- (3) Six distinct denoising methods from linear and non-linear categories were used to reduce the amount of noise in histopathology images. These methods were assessed based on the amount of noise levels they produced and the ratio of signal to noise in the filtered image compared to the original. We provide several statistical analyses and comparisons of algorithm complexity which justify our goal and objective.
- (4) Lastly, we combine the best result-giving color normalization and denoising techniques to investigate the combined effect. We also evaluate each color normalization and denoising method's output using the chosen quality evaluation metrics

This is how the rest of the article is organized. In section 2, a review of the literature is provided on the benefits and drawbacks of each color normalization and denoising technique used in this comparative analysis. The supplies and methods used in this study are presented in Section 3. To demonstrate the performance differences based on the structural similarity evaluation metrics using illustrative graphics, we conduct a comparative quality analysis of all the current algorithms in section 4. In section 5, results and discussion are displayed. Lastly, section 6 presents the conclusions of our research.

Our work broadens the scope by incorporating a thorough comparative analysis of seven color normalization methods and six denoising techniques, in contrast to other research that mostly concentrated on SSIM-based evaluations of color normalization methods. To provide a more thorough and reliable assessment, we also use three sophisticated similarity evaluation metrics (SSIM, QSSIM, and MS-SSIM) to evaluate quality preservation at various scales. While several studies research foundational knowledge and methodologies for color normalization and denoising methods [1-5], our research explicitly combines structural similarity assessment with multi-scale denoising techniques for histopathology images.

#### 2. Literature Review

To examine the structural similarity of histopathology tissue images, we select various color normalization techniques from various categories, including intensity normalization, global color normalization, color normalization following stain separation by unsupervised techniques, color decomposition, and statistical techniques. Numerous studies demonstrate that, by considering various factors, normalization techniques from different categories have diverse impacts on tissue images related to histopathology [3-5]. Histogram specification, like global color normalization techniques, can be accomplished by splitting color appearance and intensity information across multiple color spaces (RGB, HSV, and LAB) [3]. This approach methodically changes the pixel intensity value, reducing color differences while maintaining consistent color distribution. Conversely, with intensity normalization, such as min-max, we can scale the histopathological image pixel value to a particular range, like [0 to 1] or [0 to 255]. When morphological traits are preserved, min-max normalization can improve the comparability of tissue structures between different samples [7]. More influence is exerted by the color decomposition algorithms, which efficiently divide the overlap of chromogenic signals into comprehensible color channels.

Techniques for color decomposition can maintain the histopathological tissue samples' contextual and structural integrity [9]. The image can be divided into smaller blocks for statistical approaches such as CLAHE [19], and each block can then have its histogram equalization done independently [10, 11]. To separate stain color components, Macenko et al. presented one of the most used color normalizing methods based on singular value decomposition (SVD) [13]. In addition to bringing histopathology images' color variation back to normal, removing superfluous noise from the images is crucial to protecting vital cellular structures. Denoising techniques can minimize noise introduced during formation and recording, hence improving the quality of the histopathological image [14]. Several denoising techniques from several filtering categories, including multiscale, non-linear, and linear filtering, were employed in this study to enhance the comparative analysis of our prostate cancer dataset. A linear relationship between pixel values throughout the image is used in linear denoising techniques. Conversely, non-linear denoising techniques maintain the important structural elements and edges by considering the surrounding pixels' context [13-17]. A small amount of research has systematically analyzed the combined effects of color normalization and denoising techniques on histopathology images using sophisticated similarity measures like QSSIM and MS-SSIM. In contrast, earlier studies have assessed these techniques independently. Additionally, existing methods often lack statistical validation and do not incorporate multi-scale evaluation. In order to provide a thorough evaluation framework, this study fills this gap by combining several normalization and denoising algorithms, evaluating their efficacy using SSIM-based metrics, and performing statistical significance analysis.

## 3. Materials and Method

This section includes the study's materials and methodology as well as an overview of each color normalization, denoising, and similarity index metric that was chosen for the analysis of histopathology prostate cancer images.

#### 3.1 Dataset

We used a carefully selected dataset of prostate cancer images for this study from Yonsei University Severance Hospital, and the Institutional Review Board granted us access (Approval No. 1-2018-0044). With an Aperio AT2 scanner, the tissue slides were scanned at  $20 \times$  magnification, with a resolution of 0.25 µm/pixel. Initially, all slides in the dataset were classified as benign, with Gleason scores ranging from 3 to 5. To do a comprehensive analysis, we used 100 histopathological images from each range separately.

## 3.2 Structural similarity evaluation matrix

To evaluate the quality of normalization methods, we focus on three state-of-the-art structural similarity metrics including structural similarity index matrix (SSIM), quaternion structural similarity index matrix (QSSIM), and multi-scale structural similarity index matrix (MS-SSIM) of our histopathology prostate cancer image dataset.

## 3.2.1 **SSIM**

Luminance, contrast, and structure are the three major components of an image that are combined to provide structural similarity by providing a number between 0 and 1, which

represents the overall quality of the image. The normalized image and source are more comparable when the numerical value is closer to 1, whereas less similarity is indicated by the reverse [3, 20]. Both the local and global structural information of an image can be computed by SSIM. The scalar cross correlation between the original and normalized images was the only thing we considered when computing the SSIM.

Together, the three elements produced a mathematical formula that was,

$$SSIM(j,k) = [l(j,k)]^{\gamma} \cdot [c(j,k)]^{\delta} \cdot [s(j,k)]^{\lambda}$$
(1)

Luminance, contrast, and structure are denoted by the terms l(j, k), c(j, k), and s(j, k), respectively.

$$l(j,k) = \frac{2.\mu j.\mu k + C_1}{\mu^2_{j} + \mu^2_{k} + C_1}$$

$$c(j,k) = \frac{2.\sigma j.\sigma k + C_2}{\sigma^2_{j} + \sigma^2_{k} + C_2}$$

$$s(j,k) = \frac{\sigma_{jk} + C_3}{\sigma_{j}.\sigma_{k} + C_3}$$
(4)

$$c(j,k) = \frac{2.\sigma j.\sigma k + C_2}{\sigma^2 + \sigma^2 k + C_2}$$
(3)

$$s(j,k) = \frac{\sigma_{jk} + C_3}{\sigma_{j,\sigma_k} + C_3} \tag{4}$$

SSIM can be expressed as follows when all the formulas (eq 2-4) for luminance, contrast, and structure have been combined.

$$SSIM(j,k) = \frac{(2\mu_j \mu_k + C_1)(2\sigma_j \sigma_k + C_2)}{(\mu^2_j + \mu_k^2 + C_1(\sigma^2_j + \sigma^2_k + C_2)}$$
(5)

The formula defines  $\sigma_i$  and  $\sigma_k$  as the standard deviations (SDs) of the original and normalized images, respectively, with  $\mu_i$  and  $\mu_k$  representing their respective mean intensities. When the SSIM becomes close to zero,  $C_1$ ,  $C_2$ , and  $C_3$  make it stronger. The correlation coefficient between the original and normalized images is defined as  $\sigma_{ik}$ . We calculate the SSIM value, which is a number between 0 and 1, where a number closer to 1 indicates a significant similarity and a value nearer 0 indicates a significant difference between the original and normalized image.

### **3.2.2 QSSIM**

We compute the quaternion structural similarity by focusing on both scalar and crosscorrelation to assess the detailed changes between the color vectors [21]. To illustrate the quality difference between the source and processed images, QSSIM measures the size and direction of a histopathological image whereas SSIM measures the size [3].

$$QSSIM_{ref,deg} = \left| \left( \frac{2\mu_{qref}\mu_{qdeg}}{\mu_{qref}^2 + \mu_{qdeg}^2} \right) \left( \frac{\sigma_{qref,qdeg}}{\sigma_{qref}^2 + \sigma_{qdeg}^2} \right) \right|$$
 (6)

 $\mu_{qref}$  and  $\mu_{qdeg}$ , respectively, represent the sample mean and processed images. Conversely, the source and processed image standard deviations are denoted by  $\sigma_{qref}$  and  $\sigma_{qdeg}$ , respectively. The correlation coefficient  $\sigma_{qref,qdeg}$  represents the relationship between the original and normalized images.

#### 3.2.3 MS-SSIM

While single scale may be appropriate in some contexts, multi-scale methods provide a practical approach to combine image information at varying resolutions. With greater flexibility than single-scale, the multi-scale structural similarity index (MS-SSIM) breaks down the source image into many scales and computes the SSIM scores at each scale to capture both local and global similarities [22]. MS-SSIM offers a more thorough measure of similarity by considering the many scales of image structure. To evaluate the preservation of textures and fine features of our histopathology prostate cancer dataset, we apply the multi-scale approach with SSIM and QSSIM to capture and analyze the image quality across several spatial resolutions [20, 22].

The MS-SSIM formula used in our research is in conjunction with the preceding equations (eq. 1-4).

$$MS - SSIM(j,k) = [l_M(j,k)]^{\alpha_M} \cdot \prod_{i=1}^{M} [c_i(j,k) \cdot s_i(j,k)]^{\beta_i}$$
 (7)

In this equation,  $l_M(j, k)$  is the luminance comparison at the contrast scale, and  $c_i(j, k)$  and  $s_i(j, k)$  are the contrast and structure comparison at scale i. The weights  $\alpha_M$  and  $\beta_i$  are used to evaluate image quality by comparing luminance, contrast, and structure at different scales.

#### 3.3 Noise level evaluation matrix

We calculate the mean noise level by calculating the standard deviation (SD) and signal-to-noise ratio (SNR) to assess the image-denoising techniques.

## 3.3.1 SD

Images are first converted to a grayscale image, and the standard deviation (SD) of the pixel intensities in each grayscale image is then calculated to determine the noise level in the prostate cancer histopathology images [23, 24]. In grayscale images,  $I_j$  is regarded as the pixel value at the location j. N and  $\mu$  are the total number of pixels in the grayscale images and the mean pixel intensity, respectively. The equation that's applied is,

$$\mu = \frac{1}{N} \sum_{j=1}^{N} I_j \tag{8}$$

The standard deviation (SD) can be calculated using the following mathematical formula,

$$\sigma = \sqrt{\frac{1}{N}} \sum_{j=1}^{N} (I_j - \mu)^2 \tag{9}$$

To determine the amount of noise removed from the original images, we compute the mean noise level (SD) for both the original and processed images.

#### 3.3.2 SNR

Images with a stronger signal are thought to be of higher quality. The signal-to-noise ratio compares the desired signal to the amount of background noise in the image [25, 26]. SNR is used in this study to compare the signal of the prostate cancer histopathology images to the

image's background noise. The mean pixel value and the noise level are used to calculate the SNR. The equation is,

$$SNR = 10log_{10}(\frac{\mu}{\sigma}) \tag{10}$$

In this formula,  $\sigma$  is the mean noise level, which was determined using the standard deviation, and  $\mu$  denotes the mean pixel intensities.

### 3.4 Color Normalization Methods

Normalization is defined as producing an image description that is independent of the illumination circumstances under which the image was captured [27]. Our experimental methods for processing and analyzing the histopathology of prostate cancer images are derived from many normalization categories. To maintain the most significant information, these normalization techniques can improve the structural similarity between the original and normalized images. The process of histogram equalization is applied while converting an image from RGB to  $l\alpha\beta$  space, as stated in the histogram specification [6, 28]. The normalized images retain most of the brightness and color characteristics of the original images, even though the overall source information cannot be retained. Pixel values in each color channel are scaled in the min-max color normalization process so that they fall within the range. After deducting the least value from each pixel, this is accomplished by dividing each pixel by the highest value. The IRIS dataset was used in a 2017 study by Pandey and Jain to investigate data-normalizing approaches using the min-max methods. They discovered that the min-max normalization method produced 100% accuracy at k = 1 [7].

Complete color normalization can identify the source of color variation, including the illuminant and stain variance, as treating the color variation in histopathology images is an important task [8]. It can use structured weight (SW) statistics to utilize an intensity-matching technique and spectral normalization module to decrease the NMF solution space. The original image can be transformed into a saturated image by using the structured weight [8, 3]. By converting the images from RGB to Maxwellian color space, blind color decomposition helps to extract the intensity information from the color information. From the perspective of color theory, this transformation makes it possible to characterize an ideal stain and quantify stain quality [9]. Despite offering the color distribution of individual stains, this approach has the potential to create artifacts in the normalized image during processing. Using a contrastlimited adaptive histogram equalization algorithm is a well-known technique to improve the contrast of histopathological images. By clipping the contrast enhancement to a limit, this approach specifically increases the contrast of three channels (R, G, and B) in sequential order [10]. Through the process of clipping the histogram on each block, CLAHE can improve the contrast by dividing the input image into multiple equal-sized blocks [11]. The orthonormal transformation of the original RGB image to optical density—which makes staining densities possible—is typically the basis for the color deconvolution technique. This conversion facilitates the acquisition of independent data regarding the contribution of each stain to an image of histopathology. Higher computational complexity is a drawback, but it also has a benefit in that each stain's image can be rebuilt independently for densitometry and texture analysis [3, 12]. Macenko et al. proposed one of the most widely used color normalization techniques based on singular value decomposition (SVD) to separate stain color components. We include the Macenko method as a baseline in our experiments to ensure a more comprehensive comparison.

## 3.5 Denoising Methods

Due to sensor malfunctions, inadequate brightness, or incorrect correspondence during picture capture, medical images frequently contain noise [14]. In this case, denoising the images is essential to enhance the histopathological image quality for subsequent analysis, including segmentation, classification, and other medical image processing domains. In this study, we have assessed the denoising techniques we select from the linear and non-linear filter classes by calculating the prostate cancer image dataset's mean noise level and signal-to-noise ratio. The median filter, which retains edges and other crucial features [29, 30], effectively eliminates the noise present in histopathological images. Every pixel in the image should have its median value replaced by that of its neighbor [13, 14]. This technique locates the neighborhood for each pixel in the input image, after which it calculates the median value of the neighborhood. Using a Gaussian kernel that can retain the important characteristics to create a smooth image, the Gaussian filter mixes the images [14]. The weighted average of the neighborhood is calculated by the Gaussian kernel, which subsequently assigns the appropriate pixel to it. On the other hand, a bilateral filter convolves the image using a Gaussian kernel in both the spatial and intensity domains to preserve the discontinuities while blurring the image and maintaining the borders and edges [15]. However, the size of the neighborhood employed by the mean filter technique is controlled by a hyperparameter called kernel size. Every pixel in an image is replaced with the average of its neighbors using this denoising technique. In our dataset, we have opted to employ several kernel sizes for testing since it might be more appropriate to use a larger kernel size when denoising an image that is hazy and a smaller kernel size when denoising an image that is noisy but has distinct edges [14].

This technique reduces image noise by using wavelet transforms. Following the division of the image into a group of frequency subbands, thresholding is done to reduce noise in the high frequency subbands. The inverse wavelet transform should then be used to recreate the denoised image [16]. The non-local means denoising approach compares every pixel in an image inside a dataset. The filter computes the weighted average by the similarity of the pixels that are closest to the current pixel to do this comparison. First, we set up an initial filtered image with the same dimensions as the input image [17]. We analyze multiple parameters for each denoising method and change the optimal values of sigma value, threshold value, and kernel size to minimize noise while maintaining important details.

## 3.6 Integrating Normalization Method with Denoising Techniques

By integrating color normalization and image denoising methods, the most desired performance giver from both sections, we extend our comparative study based on the comparative result. We want to further investigate the structural similarity index metrics by combining these two approaches in our experiments.

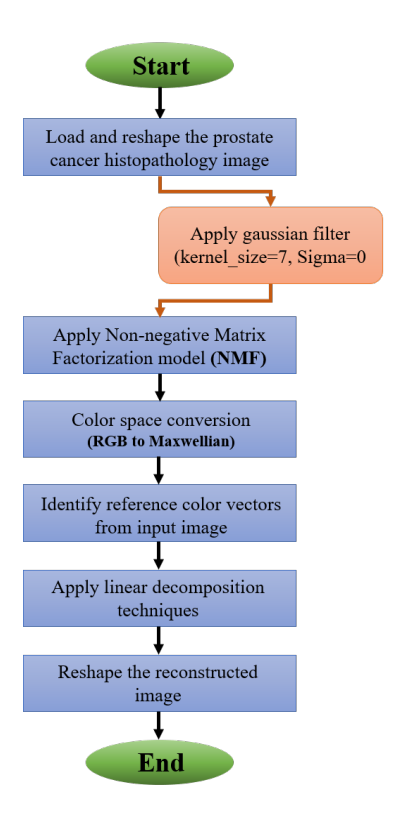


Fig. 1. Flow chart for the implementation of blind color decomposition and gaussian filter together.

**Fig. 1** shows the sequential combination implementation of the Gaussian algorithm [14] and blind color decomposition [3] for our prostate cancer histopathology image dataset, which performs better than other presented methods. To implement the gaussian algorithm, we experimented with several kernel sizes  $(3 \times 3, 5 \times 5, 7 \times 7)$ , with kernel size  $7 \times 7$  yielding the best results. In contrast, to identify patterns in images, we employ blind color decomposition, which divides an image into three color components (red, green, and blue) using the nonnegative matrix factorization (NMF) [3, 9]. Additionally, to improve the separation of spectral components and the classification and analysis task for the histopathological medical images, we transform the images to Maxwellian color space.

# 4. Comparative Analysis

The impact of the color normalization and denoising methods on tissue images from prostate cancer histopathology is assessed in the following section through a comparative quality study.

**Table 1.** Comparison of seven color normalization methods based on SSIM, QSSIM, and MS-SSIM metrics for the prostate cancer dataset. Higher values indicate better similarity preservation.

Method	SSIM	QSSIM	MS-SSIM
Histogram Specification	0.773	0.814	0.639
Min-max Normalization	0.831	0.861	0.977
Complete Color Normalization	0.828	0.850	0.969

Blind Color Decomposition	0.834	0.864	0.989
Contrast Enhancement (CLAHE)	0.797	0.833	0.781
Color Deconvolution	0.817	0.851	0.903
Macenko	0.830	0.861	0.981

Based on a comparative study of seven color normalization methods applied to one hundred histopathological prostate cancer images (Gleason scores of 3, 4, and 5) we observed that the blind color decomposition method outperforms the other methods (Table 1). In both SSIM, QSSIM, and MS-SSIM this method gives a value of 0.834, 0.864, and 0.989 respectively. We employ a non-negative matrix factorization (NMF) with three components, initialized via Nonnegative Double Singular Value Decomposition (NNDSVD), and confined to 500 iterations to develop the blind color decomposition approach. This ensures reproducibility with a fixed random state. On our dataset, the min-max, macenko, complete color, and color deconvolution algorithms also exhibit a stronger influence. Since the purpose of our study is to evaluate the structural similarity of color normalization methods on histopathology images, we selected three methods: MS-SSIM to analyze the images at different resolutions and scales, QSSIM to enhance the power of SSIM by adding perceptual quality factors, and SSIM to measure the similarity in structure, luminance, and contrast between the original and normalized images. QSSIM can improve the accuracy of diagnosis in the field of medical imaging by offering a sophisticated assessment of image quality that closely matches expert human evaluations [20, 21].

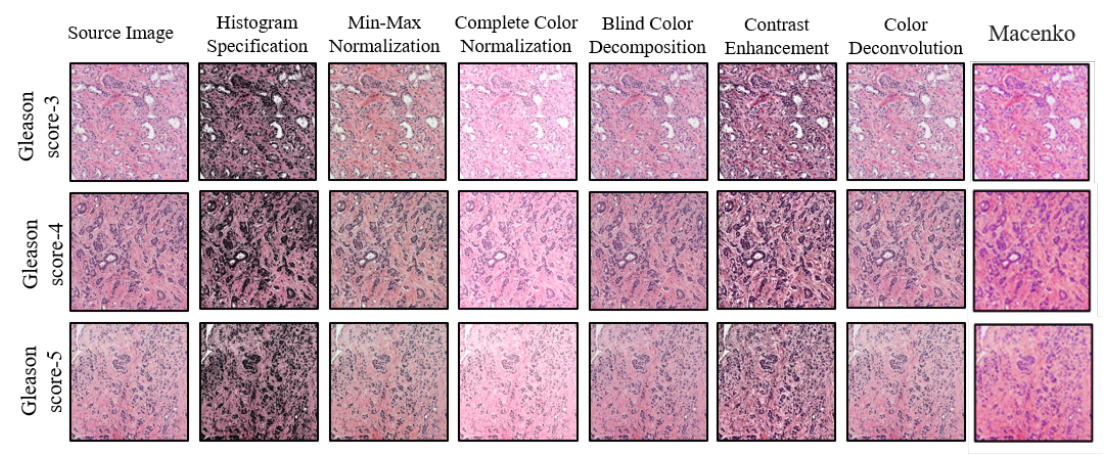


**Fig. 2.** Visualization of seven different color-normalized images from different Gleason scores for the prostate cancer image dataset. The first column is the original images while the rest of the columns represent the normalized images.

The visual contrasts between the original and normalized images from various color normalization methods are shown in Fig. 2. Three source images were selected from among 100 malignant images based on three distinct Gleason scores to present a more useful assessment of the entire prostate cancer dataset in this figure. The original/source images from Gleason scores 3, 4, and 5 are displayed in the first column.

Metric	Anova F-Value	p-Value	Significance (p<0.05)
SSIM	11.85	0.0027	Significant
QSSIM	9.94	0.0071	Significant
MS-SSIM	13.62	0.0014	Significant

**Table 2.** ANOVA (Analysis of Variance) statistical analysis for similarity metrics.

ANOVA (Analysis of Variance) determines whether the means of multiple groups—in this case, the SSIM, QSSIM, and MS-SSIM scores across different color normalization methods—are significantly different. It does this by comparing the variance between groups (differences in mean values of methods) with the variance within groups (variations within each technique). The ratio of these variances is known as the F-value, and a higher F-value shows that at least one strategy is significantly different from the others. We apply a p-value significance test and reject the null hypothesis if p < 0.05, showing a statistically significant difference between normalization methods. This statistical validation confirms that the differences in similarity scores are not random, supporting the conclusion that Blind Color Decomposition outperforms other methods (Table 2). Since all p-values are below 0.05, the observed improvements are statistically significant, strengthening the study's claims and providing justification for performance differences.

 Table 3. Computational Complexity Table (Big-O Analysis) for the normalization methods.

Normalization Method	Computational Complexity (Big-O Notation)
Histogram Specification	O(n log n)
Min-max Normalization	O(n)
Complete Color Normalization	$O(n^2)$
Blind Color Decomposition	$O(n \log n)$
Contrast Enhancement (CLAHE)	O(n)
Color Deconvolution	$O(n^2)$
Macenko Normalization	$O(n \log n)$

The computational complexity of each color normalization approach was determined by the underlying algorithmic procedures. The key operation of histogram-based transformation processes (histogram specification, blind color decomposition, and macenko) is sorting intensity values, which has an O(n log n) complexity. Methods utilizing pixel-wise transformations (Min-Max Normalization, CLAHE) involve direct intensity mapping, resulting in a more efficient O(n) complexity. Color Deconvolution which uses matrix factorization or eigenvalue decomposition, has quadratic computational complexity (O(n²)).

These complexity values were derived from algorithmic analysis rather than empirical execution times, ensuring a theoretical justification of computational feasibility for each method.

In order to balance computing efficiency with performance accuracy and to meet the paper's goal of determining the best normalization technique, it is imperative that computational complexity be taken into account in the study. Despite having the highest similarity scores, Blind Color Decomposition is a strong contender for practical implementation because of its (O(n log n)) trade-off between performance and efficiency (Table 3). By presenting both accuracy metrics (SSIM, QSSIM, MS-SSIM) and computational feasibility (Big-O complexity), the study provides a holistic evaluation that helps researchers choose a method suited for scalable and high-quality histopathology image analysis.

**Table 4.** Comparison of six image denoising methods based on mean noise level, standard deviation, and signal-to-noise ratio (SNR) for the prostate cancer dataset. Higher SNR values indicate better noise reduction, with the best-performing method in bold.

Method	Original noise level	Processed image's noise level	Percentage of noise reduction	Original SNR (dB)	Processed SNR (dB)
Median		25.844	33.67%		8.39
Gaussian		25.542	34.44%		8.46
Bilateral		33.205	14.7%		7.22
Mean	38.961	29.824	23.45%	6.50	7.68
Wavelet Transform-based		34.793	10.70%		3.33
Non-local Means		35.364	9.23%		6.95

In this work, we assess both linear and non-linear denoising techniques to provide a thorough analysis and comparative assessment of the effects of denoising techniques on histopathological images. **Table 4** demonstrates that the Gaussian filter outperforms the others in terms of noise reduction, with a reduction of 34.44%. The noise level in the original and filtered images is 38.961 and 25.542, respectively. Conversely, the SNR value obtained from this approach is 8.46 dB, while the SNR value from the original image was 6.50 dB. The percentage indicates that compared to the original and other filtered images from different techniques, the Gaussian-filtered images have substantially less noise. Additionally, considering the signal-to-noise ratio, the growing SNR value demonstrates that the Gaussian-filtered images are 8.46 dB stronger than the original images. After examining several factors and parameters, we decided on the kernel size  $(7 \times 7)$  to achieve the best results when implementing the Gaussian filter. Additionally, the standard deviation in the x direction (sigma\_x = 0), where the function can compute the standard deviation automatically based on the kernel size when the sigma value is zero. The median and mean filter also have a closer impact on our dataset according to their percentage of noise reduction and signal-to-noise ratio.

In **Fig. 3**, the signal-to-noise ratio and noise level are shown using three distinct dimensions for easier comprehension. The evaluation metrics (SNR and standard deviation), the denoising techniques, and the value are stored on these three axes. This figure clearly illustrates how the highest degree of SNR is increased, and the highest level of noise is reduced when using a Gaussian filter. Even the Gaussian filter reduces the highest percentage of noise compared to other methods. To achieve the best result for noise reduction in each denoising approach, we look at every conceivable parameter. The rationale behind selecting the linear, non-linear, and

multi-scale denoising approaches to optimally evaluate the prostate cancer dataset.

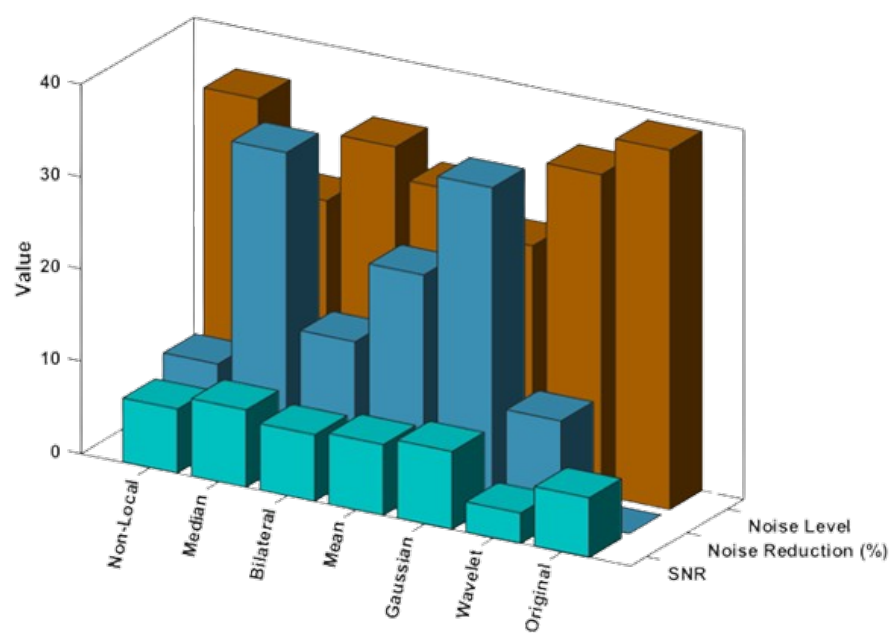


**Fig. 3.** A three-dimensional graph showing, for the selected image denoising techniques, the relative differences between the original and filtered images based on their mean noise level, signal-to-noise ratio, and percentage of noise reduction.

The precise parameters and values that we used to apply the chosen denoising techniques are listed in **Table 5**. We examined various kernel widths, sigma values, threshold values, and other factors to apply these algorithms in a way that would minimize potential noise and enhance the image based on the signal-to-noise ratio. Ultimately, the quantities listed in **Table 5** provide the best outcome that is both desired and feasible. We also experimented with these denoising methods with specific parameters with all the present color normalization methods to see the differences in structural similarity index metrics.

**Table 5.** Specific parameters with their specific values to implement the selected denoising techniques after analyzing several values to get the desired outcome.

Method	Parameter	Range
Median	kernel size	5 × 5
Gaussian	Kernel size	7 × 7
Gaussian	sigma	0
	diameter	9
Bilateral	sigma Color	75
	sigma Space	75
Mean	Kernel size	3 × 3
Wavelet Transform-based	kernel size	5 × 5
wavelet Transform-based	threshold value	200
	luminance component	10
Non-local Means	color components	10
Non-local Means	template Window	7 × 7
	Search Window	21 × 21

### 5. Result and Discussion

In this section, we performed a combination of color normalization and denoising methods for our prostate cancer dataset to see whether any changes happened or not in the three structural similarity metrics of our histopathology prostate cancer dataset. The quantitative results of color normalization and image denoising from **Table 1** and **Table 4** show that the blind color decomposition and Gaussian methods have a greater impact compared to other methods.

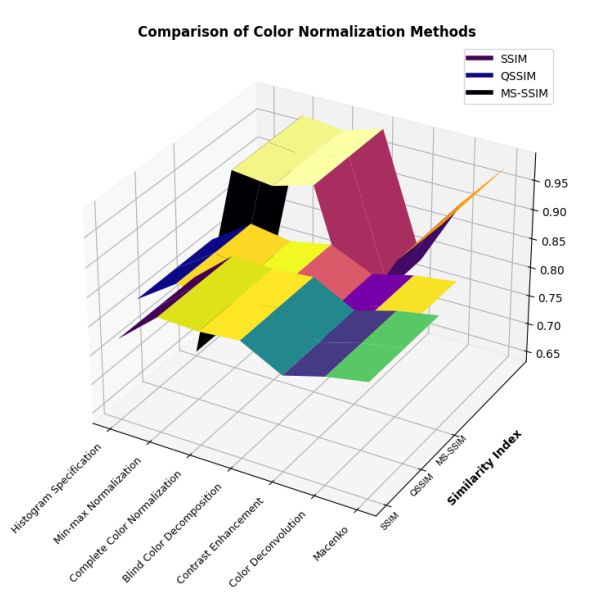


**Fig. 4.** Three-dimensional (3D) colormap to visualize the impact of color normalization methods based on the structural similarity indices.

The efficacy of six distinct color normalizing techniques is compared in a 3D surface plot shown in Fig. 4 based on the selected method, Histogram Specification, Min-max normalizing, Complete Color Normalization, Blind Color Decomposition, Contrast Enhancement, Color Deconvolution, and Macenko. The structural similarity index (SSIM), the multi-scale structural similarity index (MS-SSIM), and the quaternion structural similarity index (QSSIM) are the evaluation metrics that are employed. The color normalization techniques are represented by the X-axis, while the similarity indices are categorized by the Y-axis. The values of SSIM, QSSIM, and MS-SSIM are indicated on the Z-axis. The 'viridis' colormap uses the SSIM data to show how well each method preserves image structure. Structural similarity is quantitatively evaluated by the QSSIM values, which are displayed on the 'plasma' colormap. The 'inferno' colormap represents the MS-SSIM values, which quantify the structural similarity at various scales and offer a thorough assessment of the image quality after normalization.

In the present study, Blind Color Decomposition exhibits the highest performance in maintaining the structural similarity of the image, displaying the most significant values in SSIM, QSSIM, and MS-SSIM. As shown by its high efficacy, particularly in the MS-SSIM metric, min-max normalization, and macenko additionally shows potential for multi-scale structure preservation. This three-dimensional map shows how different color normalizing methods impact the image's structural similarity and allows for a clear and comprehensive comparison of the methods using multiple similarity indexes. With different colormaps for

each metric, the readability and distinction between the similarity indices are enhanced.

**Table 6.** Comparative analysis on the impact of denoising methods in combination with color normalization method for the prostate cancer image dataset. Comparatively, the impact of combining Gaussian denoising methods with the blind color decomposition method is shown in bold font.

Method	SSIM	QSSIM	MS-SSIM
Blind Color Decomposition (without Gaussian)	0.834	0.864	0.989
Blind Color Decomposition (with Gaussian)	0.857	0.884	0.998

Table 6 provides a detailed comparison of the performance of Blind Color Decomposition (BCD) in two different configurations: without Gaussian filtering and with Gaussian filtering. Each indicator offers a unique perspective on how well the color normalization technique preserves the images' structural and artistic integrity. The table clearly shows that an SSIM value of 0.857 is obtained when Gaussian filtering is used in conjunction with BCD. This value is higher than the 0.834 value obtained when filtering is not used. This implies that the structural preservation including the luminance, contrast, and structure of the images is enhanced using Gaussian filtering. The QSSIM value of 0.884 produced by blind color decomposition with Gaussian filtering is greater than the 0.864 obtained in the absence of Gaussian filtering. With this improvement, Gaussian filtering more effectively preserves the color and structural integrity of the quaternion space, leading to a more accurate representation of the image's similarity. The enhancement in MS-SSIM, with a 0.998 score, indicates how effectively it maintains image characteristics across various scales, resulting in enhanced overall image quality. Table 6 clearly shows that, for all three similarity standards, Blind Color Decomposition performs significantly better when Gaussian filtering is applied with certain parameters (Table 5). These results show the value of Gaussian filtering in color normalization and its capacity to maintain the aesthetic and structural integrity of normalized images.

### 6. Conclusion

This study uses various color-normalizing methods to provide a comparative evaluation of the structural similarity of prostate cancer histopathology images. Three distinct similarity metrics are used to evaluate structural similarity: the multi-scale structural similarity index matrix (MS-SSIM), the quaternion structural similarity index matrix (QSSIM), and the structural similarity index matrix (SSIM). The objective of our analysis was to examine the overall structural similarity of histopathological images from all angles, including the structure, size, direction, brightness, contrast, and numerous scales of an image by implementing different types of color normalization methods. To minimize potential noise in histopathology images, we also examine various linear, non-linear, and multi-scale filtering algorithms. Throughout the experiment, it becomes evident that the Gaussian filter and blind color decomposition have a significant impact on our prostate cancer dataset, providing the largest percentage of noise reduction and the highest similarity for all similarity metrics, respectively. When we combine the blind color decomposition with a Gaussian filter that has characteristics, this experimental comparison even works better. With this combined implementation, our prostate cancer images' structural similarity increases significantly across all structural

similarity evaluation parameters. This study demonstrates the significant influence of color decomposition techniques on histopathology image processing, particularly on images of prostate cancer. By comparing color normalization and denoising techniques, we want to advance the fields of medical image analysis and computer-aided clinical diagnosis.

# **Acknowledgment**

Conflict of Interest: The authors declare that they have no conflict of interest.

Availability of Data and Materials: The data set used in this study is private.

**Authors' Contributions:** All authors equally contributed to the article.

#### References

- [1] Vahadane, A., Peng, T., Sethi, A., Albarqouni, S., Wang, L., Baust, M., Steiger, K., Schlitter, A. M., Esposito, I., & Navab, N., "Structure-Preserving Color Normalization and Sparse Stain Separation for Histological Images," *IEEE Transactions on Medical Imaging*, vol.35, no.8, pp.1962-1971, 2016. <a href="https://doi.org/10.1036/journal.com/">Article (CrossRef Link)</a>)
- [2] Goyal, B., Dogra, A., Agrawal, S., Sohi, B. S., & Sharma, A., "Image denoising review: From classical to state-of-the-art approaches," *Information Fusion*, vol.55, pp.220-244, 2020.

  Article (CrossRef Link)
- [3] Roy, S., kumar Jain, A., Lal, S., & Kini, J., "A study about color normalization methods for histopathology images," *Micron*, vol.114, pp.42-61, 2018. <u>Article (CrossRef Link)</u>
- [4] Michielli, N., Caputo, A., Scotto, M., Mogetta, A., Pennisi, O. A. M., Molinari, F., Balmativola, D., Bosco, M., Gambella, A., Metovic, J., Tota, D., Carpenito, L., Gasparri, P., and Salvi, M., "Stain normalization in digital pathology: Clinical multi-center evaluation of image quality," *Journal of Pathology Informatics*, vol.13, 2022. <u>Article (CrossRef Link)</u>
- [5] Yee, W. C., Jian, T. X., Rahman, K. S. A., Hoe, T. L., Min, L. J., Hang, Q. Y., and Ling, T. C., "Performance Analysis of Color Normalization Methods in Histopathology Images," in *Proc. of the 2022 IEEE International Conference on Automatic Control and Intelligent Systems (I2CACIS)*, pp.147-151, IEEE, 2022. Article (CrossRef Link)
- [6] Thomas, G., Flores-Tapia, D., & Pistorius, S., "Histogram Specification: A Fast and Flexible Method to Process Digital Images," *IEEE Transactions on Instrumentation and Measurement*, vol.60, no.5, pp.1565-1578, 2011. Article (CrossRef Link)
- [7] Henderi, H., Wahyuningsih, T., & Rahwanto, E., "Comparison of Min-Max normalization and Z-Score Normalization in the K-nearest neighbor (kNN) Algorithm to Test the Accuracy of Types of Breast Cancer," *International Journal of Informatics and Information Systems*, vol.4, no.1, pp.13-20, 2021. <a href="Article">Article</a> (CrossRef Link)
- [8] Li, X., & Plataniotis, K. N., "A Complete Color Normalization Approach to Histopathology Images Using Color Cues Computed From Saturation-Weighted Statistics," *IEEE Transactions on Biomedical Engineering*, vol.62, no.7, pp.1862-1873, 2015. <a href="https://example.com/Article/Article/CrossRef Link">Article (CrossRef Link)</a>)
- [9] Gavrilovic, M., Azar, J. C., Lindblad, J., Wählby, C., Bengtsson, E., Busch, C., & Carlbom, I. B., "Blind Color Decomposition of Histological Images," *IEEE Transactions on Medical Imaging*, vol.32, no.6, pp.983-994, 2013. <a href="https://example.com/Article/Article/CrossRef Link">Article (CrossRef Link)</a>
- [10] Sonali, Sahu, S., Singh, A. K., Ghrera, S. P., & Elhoseny, M., "An approach for de-noising and contrast enhancement of retinal fundus image using CLAHE," *Optics & Laser Technology*, vol.110, pp.87-98, 2019. <a href="https://doi.org/10.1001/journal.com/">Article (CrossRef Link)</a>)

- [11] Ojo, J. A., Solomon, I. D., & Adeniran, S. A., "Contrast enhancement algorithm for colour images," in *Proc. of the 2015 Science and Information Conference (SAI)*, pp.555-559, IEEE, Jul. 2015. Article (CrossRef Link)
- [12] Islam, T., M., Al-Shidaifat, A., Jooq, M. K. Q., & Song, H., "Ultra-Efficient Low-Power Retinal Nano Electronic Circuit for Edge Enhancement and Detection Using 7 nm FinFET Technology," *Journal of Nanoelectronics and Optoelectronics*, vol.19, no.6, pp.573-587, 2024. Article (CrossRef Link)
- [13] Macenko, M., Niethammer, M., Marron, J. S., Borland, D., Woosley, J. T., Guan, X., Schmitt, C., & Thomas, N. E., "A method for normalizing histology slides for quantitative analysis," in *Proc. of the 2009 IEEE International Symposium on Biomedical Imaging: From Nano to Macro*, pp.1107-1110, 2009. <a href="https://doi.org/10.1007/journal.com/">Article (CrossRef Link)</a>
- [14] Ahamed, B. B., Yuvaraj, D., & Priya, S. S., "Image Denoising With Linear and Non-linear Filters," in *Proc. of the 2019 International Conference on Computational Intelligence and Knowledge Economy (ICCIKE)*, pp.806-810, IEEE, Dec. 2019. Article (CrossRef Link)
- [15] Chen, B.-H., Tseng, Y.-S., & Yin, J.-L., "Gaussian-Adaptive Bilateral Filter," *IEEE Signal Processing Letters*, vol.27, pp.1670-1674, 2020. <u>Article (CrossRef Link)</u>
- [16] Hossain, I., & Moussavi, Z., "An overview of heart-noise reduction of lung sound using wavelet transform based filter," in *Proc. of the 25th Annual International Conference of the IEEE Engineering in Medicine and Biology Society (IEEE Cat. No.03CH37439)*, vol.1, pp.458-461, IEEE, Sep. 2003. <a href="https://doi.org/10.1001/jeep.
- [17] Buades, A., Coll, B., & Morel, J.-M., "Non-Local Means Denoising," *Image Processing On Line*, vol.1, pp.208-212, 2011. <u>Article (CrossRef Link)</u>
- [18] Ikromjanov, K., Bhattacharjee, S., Sumon, R. I., Hwang, Y.-B., Rahman, H., Lee, M.-J., Kim, H.-C., Park, E., Cho, N.-H., & Choi, H.-K., "Region Segmentation of Whole-Slide Images for Analyzing Histological Differentiation of Prostate Adenocarcinoma Using Ensemble EfficientNetB2 U-Net with Transfer Learning Mechanism," *Cancers*, vol.15, no.3, 2023. Article (CrossRef Link)
- [19] Rabeya, R. A., Uddin, S. M. I., Chowdhury, K. H., Choi, H.-K., & Kim, H.-C., "DeepLesionNet: Precise Segmentation and Classification of Skin Lesions via Convolutional Neural Networks," *Journal of the Korea Institute of Information and Communication Engineering*, vol.29, no.2, pp.149-160, 2025. Article (CrossRef Link)
- [20] Wang, Z., Bovik, A. C., Sheikh, H. R., & Simoncelli, E. P., "Image quality assessment: from error visibility to structural similarity," *IEEE Transactions on Image Processing*, vol.13, no.4, pp.600-612, 2004. Article (CrossRef Link)
- [21] Kolaman, A., & Yadid-Pecht, O., "Quaternion Structural Similarity: A New Quality Index for Color Images," *IEEE Transactions on Image Processing*, vol.21, no.4, pp.1526-1536, Apr. 2012. Article (CrossRef Link)
- [22] Wang, Z., Simoncelli, E. P., & Bovik, A. C., "Multiscale structural similarity for image quality assessment," in *Proc. of the Thrity-Seventh Asilomar Conference on Signals, Systems & Computers*, 2003, vol.2, pp.1398-1402, IEEE, Nov. 2003. <a href="https://example.com/Article/Proceedings of the Introduction of the Intro
- [23] Xie, H., Yi, S., & Yang, Z., "A Robust Noise Estimation Algorithm Based on Redundant Prediction and Local Statistics," *Sensors*, vol.24, no.1, 2024. <a href="https://example.com/Article/Article/CrossRef Link">Article/CrossRef Link</a>)
- [24] Rabeya, R. A., Bhattacharjee, S., Kim, D., Kim, H.-C., Cho, N.-H., & Choi, H.-K., "An Experimental Comparison and Quantitative Analysis on Conventional Stain Normalization for Histopathology Images," *Journal of the Korea Multimedia Society*, vol.27, no.11, pp.1268-1288, 2024. <a href="https://doi.org/10.1007/j.nc.11"><u>Article (CrossRef Link)</u></a>
- [25] Welvaert, M., & Rosseel, Y., "On the Definition of Signal-To-Noise Ratio and Contrast-To-Noise Ratio for fMRI Data," *PLoS ONE*, vol.8, no.11, 2013. <u>Article (CrossRef Link)</u>
- [26] Goormaghtigh, E., "Infrared imaging in histopathology: is a unified approach possible?," *Biomedical Spectroscopy and Imaging*, vol.5, no.4, pp.325-346, 2016. <u>Article (CrossRef Link)</u>
- [27] Cernadas, E., Fernandez-Delgado, M., González-Rufino, E., & Carrión, P., "Influence of normalization and color space to color texture classification," *Pattern Recognition*, vol.61, pp.120-138, 2017. Article (CrossRef Link)

- [28] Pontalba, J. T., Gwynne-Timothy, T., David, E., Jakate, K., Androutsos, D., & Khademi, A., "Assessing the Impact of Color Normalization in Convolutional Neural Network-Based Nuclei Segmentation Frameworks," Frontiers in Bioengineering and Biotechnology, vol.7, 2019. <u>Article (CrossRef Link)</u>
- [29] Yu, J., Tan, L., Zhou, S., Wang, L., & Wang, C., "Image Denoising Based on Adaptive Fractional Order Anisotropic Diffusion," *KSII Transactions on Internet and Information Systems (TIIS)*, vol.11, no.1, pp.436-450, 2017. Article (CrossRef Link)
- [30] Ming, J., Yi, B., Zhang, Y., & Li, H., "Low-dose CT Image Denoising Using Classification Densely Connected Residual Network," *KSII Transactions on Internet and Information Systems* (TIIS), vol.14, no.6, pp.2480-2496, 2020. Article (CrossRef Link)



**Rubina Akter Rabeya** currently continuing her PhD in Artificial Intelligence in Healthcare at Inje University. She completed her bachelor's degree in computer science and engineering from the International University of Business Agriculture and Technology (IUBAT) in 2021. Later, she received a Brain Korea (BK21) scholarship to pursue her master's degree in Artificial Intelligence in Healthcare, Inje University, South Korea in the year of 2023. Her areas of interest include artificial intelligence, XAI, medical image processing, natural language processing, and computer vision etc.



**Nam Hoon Cho** received his Master's degree in 1989 and Ph. D. in 1995 from Yonsei University in Korea after graduating from the same university in 1986. He has been a professor at Yonsei University since 1995. His major is a pathologist in genitourinary and gynecologic cancer, specialized in proteomics and multiple IHC analysis, as well as artificial intelligence based on digital image construction. He published more than 200 influential articles and more than 30 inventions.



**Hee-Cheol Kim** BSc at the Department of Mathematics, MSc at the Department of Computer Science at SoGang University in Korea, and Ph. D. at in Numerical Analysis and Computer Science at Stockholm University in Sweden. He is a professor and Head of the Department of the Institute of Digital Anti-Aging Healthcare, Inje University, South Korea. His research interests include Machine Learning, Text Mining, and Bioinformatics.



**Heung-Kook Choi** is an emeritus professor of Computer Engineering at Inje University and operates the Medical Image Technology Laboratory (MITL). In 1988 and 1990, he received his Bachelor of Engineering and Master of Engineering from Linköping University in Sweden, and his Ph.D. from Uppsala University in 1996. He served as the President of the Academy and Industry Cooperation Foundation and Dean of Research Affairs at Inje University, Korea, from 2006 to 2010. He was the president of the Koran Multimedia Society in 2013. He is interested in computer graphics, multimedia, image processing, and analysis.